Retrieving Tropospheric Temperature and Humidity Profiles Over the Ocean Using Buoy-Based Microwave Radiometers

Zhiqian Li[1,2], Fuqing Liu[1,2], Shuo Jiang[1,2], Zhongling Zhou[1,2], Zhijin Qiu[1,2], Jing Zou[1,2], Tong Hu[1,2], Ke Qi[1,2], Bo Wang[1,2]✉, Bin Wang[2,3]✉

[1]State Key Laboratory of Physical Oceanography, Institute of Oceanographic Instrumentation, Qilu University of Technology (Shandong Academy of Sciences), Qingdao, 266061, China
~~[2]Institute of Oceanography instrumentation, Qilu University of Technology (Shandong Academy of Science), Jinan, 250353, China~~
[2,3]School of Information Science and Technology, Qingdao University of Science and Technology, Qingdao, 266061, China
Correspondence to: Bo Wang (bob80.wang@hotmail.com), Bin Wang (18661855732@163.com)

Abstract. The acquisition of atmospheric temperature and humidity profiles over the sea is strategically vital for meteorological forecasting, marine monitoring, and national security. Achieving their real-time, stable, and routine retrieval under complex sea conditions is a critical and urgent challenge. Traditional retrieval methods rely heavily on large historical datasets. However, marine sounding stations are sparse, making data acquisition challenging. Ground-based microwave radiometers offer a unique capability for continuous, all-weather remote sensing of atmospheric thermal emission, enabling routine retrieval of temperature and humidity profiles over oceanic regions. Meanwhile, buoy platforms experience wave disturbance, causing real-time variations in zenith angle observations. Without correction, this induces significant random errors in target brightness temperature. To address these issues, this paper proposes a collaborative retrieval method. This method does not rely on large-scale historical datasets for model training and integrates platform attitude information. Our approach uses a multi-objective genetic algorithm to construct a small-scale joint prior database based on a limited amount of local radiosonde data, which serves only as an initial physical constraint for the retrieval process. It also incorporates an attitude error correction model, ~~a pressure-altitude model~~ an empirical pressure-altitude equation, and a parallel optimization strategy. This thereby reduces dependence on extensive historical datasets. It also effectively mitigates systematic errors from buoy attitude, enhances computational efficiency, and enables real-time, routine retrieval of marine atmospheric profiles. Simulation experiments and field tests in Qingdao's Jiaozhou Bay confirm the results. Under sparse data conditions, the temperature RMSE is 2.08 K, and the humidity RMSE of 20.95%. This validates the method's stability and applicability in real marine environments. This research provides a potentially practical pathway for ocean areas with sparse radiosondes for real-time, stable, and routine detection of marine atmospheric parameters.

批注 [清清1]: Affiliation Update: Updated and consolidated author affiliations on the title page to accurately reflect current official institutional names and organizational structures (e.g., the integration of the State Key Laboratory of Physical Oceanography and the Institute of Oceanographic Instrumentation as per current official records).

批注 [清清2]: Thank you for this comment. In the revised manuscript (Abstract, Page 1, Lines 12–14), we added a sentence linking the scarcity of routine oceanic observations with the capability of microwave radiometers to provide continuous all-weather temperature and humidity profile retrievals.
(RC1, Line 11)

批注 [清清3]: Thank you for this comment. In the revised manuscript, we clarified the role of radiosonde data in both the Abstract (Page 1, Lines 16–19) and Section 3.3.2 (Page 11, Lines 246–248). We clarified that only a limited amount of local radiosonde data is used to construct the prior database, and that no historical data input is required during the subsequent online retrieval stage.
(RC1, Line 16)

批注 [清清4]: Thank you for this comment. In the revised manuscript, we clarified that the "pressure–altitude model" refers to an empirical pressure–altitude equation. The wording has been revised in the Abstract (Page 1, Line 20), and the description of Eq. (3) has been updated in Section 3.3.1 (Page 10, Lines 231–244) to document its empirical formulation and reference source.
(RC1, Line 18)

1 Introduction

The lower troposphere is the region where most human activities and weather phenomena take place. The systematic measurement of meteorological parameters in this region is a critical foundation for high-precision weather forecasting and climate change research. It is also essential for ensuring the efficiency of aviation, ~~voyage~~ travel, and radio communication systems (Maciejewska, 2025; Morbidelli et al., 2011). However, ~~unprecedented challenges are presented for the precise detection of atmospheric parameters due to the unique geographical characteristics and dynamic processes of the marine environment.~~ the precise detection of atmospheric in the marine environment is further complicated by its unique geographical characteristics and dynamic processes. Recent studies have further highlighted the complexity of marine atmospheric structures, particularly under extreme weather conditions such as tropical cyclones (Guimond et al., 2018; Ahern et al., 2019). For instance, Wei et al. (2025) demonstrated that vertical wind shear can induce significant asymmetry in atmospheric duct distributions, underscoring the spatial and temporal variability of atmospheric properties in oceanic regions.

The primary bottlenecks are the sparse distribution of oceanic sounding stations and the inherent limitations of traditional atmospheric retrieval methods, contributing to a significant observational gap in the atmospheric boundary layer (Cimini et al., 2020). ~~Data acquisition is made extremely difficult by the sparse distribution.~~ This sparse distribution of stations makes data acquisition in the marine environment extremely difficult. The limitations are particularly evident when dealing with marine dynamic environments. ~~Specifically, these limitations include an excessive reliance on large amounts of historical data and an inability to effectively account for potential interference and correction issues. These issues are caused by changes in the attitude of the detection platform on observational signals.~~ Specifically, data-driven retrieval methods such as statistical and neural-network-based approaches exhibit strong dependence on large historical datasets, which are difficult to obtain in marine environments. In addition, buoy-based platforms are subject to wave-induced motion, which leads to variations in the observation zenith angle and consequently introduces brightness temperature deviations. These attitude-related effects must be addressed through appropriate measurement preprocessing and correction procedures before the retrieval stage.

Currently, various mainstream methods are used for atmospheric parameter profiling retrieval. These include the Bayesian maximum probability estimation algorithm (Clough et al., 2005), one-dimensional variational retrieval methods (Hewison, 2007), physically based retrieval methods based on radiative transfer theory (Zhou et al., 2024; Liu et al., 2024; Gaffard and Hewison, 2003; Reinhardt et al., 2009), and statistical retrieval methods (Zheng, 2010). Neural-network algorithms have also gained increasing attention (Renju et al., 2023). While high computational accuracy can theoretically be achieved with physical retrieval methods, their inherently large computational requirements severely limit real-time performance. Statistical retrieval methods are effective in terrestrial environments where sufficient data is available. However, their strong reliance on historical data makes them struggle in marine regions with limited data. Neural-network algorithms demonstrate outstanding performance due to their powerful nonlinear mapping capabilities. However, traditional neural network models, such as the classic backpropagation (BP)~~BP~~ neural network, generally require a large amount of training data (Hu et al., 2023; Jiménez and Eriksson, 2016). This high data requirement conflicts sharply with the limited ability to obtain field data in the unique

批注 [滴滴5]: Thank you for pointing this out. In the revised manuscript (Page 2, Line 30), "voyage" has been replaced with "travel".
(RC1, Line 27)

批注 [滴滴6]: Thank you for this comment. In the revised manuscript (Page 2, Lines 31–32), "unprecedented challenges" has been removed and replaced with a more neutral description of the additional complexity of atmospheric parameter detection in marine environments.
(RC1, Line 28)

批注 [滴滴7]: Thank you for this comment. In the revised manuscript (Page 2, Line 34), we added literature references to support the statement on the dynamical and thermodynamical complexity of the marine atmospheric boundary layer under extreme weather conditions.
(RC1, Line 31)

批注 [滴滴8]: Thank you for this comment. In the revised manuscript (Page 2, Line 39), the wording has been revised to clarify that the sparse distribution refers to the limited spatial coverage of oceanic sounding stations.
(RC1, Line 36)

批注 [滴滴9]: Thank you for this comment. In the revised manuscript (Page 2, Lines 40–45), we clarified the distinction between physics-based retrieval methods and data-driven methods, replaced the vague term "interference" with a description based on brightness temperature deviations caused by platform attitude variations, and clarified that attitude-related effects are corrected during measurement preprocessing rather than within the NSGA-II retrieval framework.
(RC1, Line 38)

批注 [滴滴10]: Thank you for pointing this out. In the revised manuscript (Page 2, Line 55), the first occurrence of "BP" has been revised to "backpropagation (BP) neural network".
(RC2, Line 49)

environment of the ocean. As a result, their training effects and retrieval performance are significantly limited (Yao and Guan, 2022; Mahdianpari et al., 2021). ~~Previous studies have confirmed this point. For example, Turner et al. (2007) noted that physical retrieval methods, while accurate, are inefficient. Decker et al. (1978) made significant progress in ground-based detection. However, the adaptability of their method in marine environments remains a key concern. Guiraud et al. (1979) revealed the detection capabilities of absorption spectra at different frequencies. In their Arctic region study, Candlish et al. (2012) explicitly pointed out that the accuracy of ship-based platform data is significantly reduced when using traditional neural-network-based retrieval of atmospheric profiles.~~ Early pioneering studies established the fundamental capabilities of ground-based microwave radiometry. For instance, Decker et al. (1978) made significant progress in ground-based detection, and Guiraud et al. (1979) revealed the detection capabilities of absorption spectra at different frequencies. However, applying these traditional methods to complex marine environments presents significant challenges. More recently, Turner et al. (2007) noted that physical retrieval methods, while accurate, are computationally inefficient for real-time applications. Furthermore, in their Arctic region study, Candlish et al. (2012) explicitly pointed out that the accuracy of ship-based platform data is significantly reduced when using traditional neural-network-based retrieval of atmospheric profiles. This is due to changes in attitude and insufficient on-site data. Recent studies also suggest that even state-of-the-art reanalysis data like ERA5 may exhibit systematic biases under complex marine weather conditions such as tropical cyclones (Wei et al., 2025), further emphasizing the need for observation-driven profiling methods in data-sparse oceanic environments. ~~These studies collectively highlight a core issue: how to effectively overcome errors caused by platform attitude and achieve high-precision, high-efficiency retrieval of atmospheric parameter profiles.~~ These studies collectively highlight a core issue: how to effectively overcome errors caused by platform attitude and achieve high-precision, high-efficiency retrieval of atmospheric parameter profiles. Although mechanical stabilization (Schnitt et al., 2024) can reduce platform motion, it introduces significant challenges for long-term autonomous buoy operation in terms of power consumption and maintenance complexity. Therefore, this study adopts a software-based approach using real-time zenith angle correction from attitude sensors. During field experiments, the buoy exhibited residual pitch and roll variations of approximately ±2.5° and ±3.2°, respectively. Our algorithm explicitly compensates for these residual pointing variations, enabling accurate retrieval of atmospheric parameters under dynamic marine conditions.

~~In this context, ground-based microwave radiometers (MWR) have emerged as a cutting-edge remote sensing technology.~~ As discussed previously, ground-based microwave radiometers (MWR) provide a powerful remote sensing technology. They are capable of capturing atmospheric microwave radiation information in real-time and continuously. This enables the retrieval of key parameters, such as atmospheric temperature and humidity profiles, and atmospheric refractive index. On the other hand, buoys are flexible, real-time monitoring platforms. They can integrate multi-parameter measurement functions and offer the unique advantages of long-term, uninterrupted, and all-weather operation. This can effectively compensate for the observational deficiencies caused by the sparse distribution of traditional oceanic sounding stations (Roemmich et al., 2009; Cronin et al., 2023; Liu et al., 2019; Fang, 2018). Consequently, an effective approach to addressing the scarcity of tropospheric data in marine environments is the combination of advanced ground-based microwave radiometer technology with ~~flexible~~

批注 [滴滴11]: Thank you for this comment. In the revised manuscript (Pages 2–3, Lines 58–64), the literature discussion has been reorganized to follow a chronological order, with early foundational studies introduced first, followed by more recent developments.
(RC1, Line 53)

批注 [滴滴12]: Thank you for this comment. In the revised manuscript (Page 3, Lines 67–74), we added an engineering justification for not adopting mechanical stabilization and provided a quantitative characterization of the residual pointing variability. We clarified that a software-based correction using attitude sensor measurements is applied, and typical residual pitch and roll variations (about ±2.5° and ±3.2°) are corrected through zenith-angle compensation.
(RC1, Line 61)

批注 [滴滴13]: Thank you for this comment. In the revised manuscript (Page 3, Line 75), the paragraph has been revised to improve continuity with the preceding discussion, including the addition of a transitional phrase to indicate that microwave radiometers were introduced earlier in the manuscript.
(RC1, Line 63)

autonomous, multi-parameter buoy monitoring platforms. Industry initiatives have previously explored this potential, such as the deployment of the first floating microwave radiometer (Haun, 2017). In the academic field, several studies have also explored the application of microwave radiometers in marine environments. For instance, Schnitt et al. (2024) and Griesche et al. (2020) demonstrated ship-based profiling capabilities, while Yan et al. (2022) focused on improving retrieval algorithms for ocean-based platforms. More recently, Cimini et al. (2025) reviewed the capability of microwave radiometers for offshore wind energy applications, highlighting that while onshore retrievals show high correlation (>0.9) with radiosondes (Cimini et al., 2003), offshore retrievals are significantly challenged by platform motion and data sparsity, necessitating advanced calibration and elevation scanning strategies.

Therefore, this study deploys a ground-based microwave radiometer on an ocean buoy platform. Through incorporating platform attitude correction methods and applying multi-objective optimization algorithms, a history-independent retrieval model is constructed to address the challenges above. Through simulation experiments and field sea trials, the method's performance, retrieval accuracy, and universality are comprehensively evaluated. Its potential for application in real marine environments is also assessed.

2 Instrument, Platform, and Sites

2.1 The QFW-6000 microwave radiometric profiler

The QFW-6000 microwave radiometer, developed by the China Electronics Technology Corporation No.22 Research Institute, is employed in this study (CETC-22, 2022; Zhang et al., 2025). The microwave radiometer is installed on the buoy's upper platform. It is used to detect, receive, and analyze microwave brightness temperatures from the zenith direction. Brightness temperature is observed from the zenith direction using 16 microwave channels. Of these, eight channels in the K-band (22.24–31.4 GHz) are primarily used to detect water vapor. ~~Eight channels in the V-band (51.26–58.0 GHz) are used to detect atmospheric oxygen.~~ Eight channels in the V-band (51.26–58.0 GHz) exploit the absorption of the oxygen to retrieve atmospheric temperature profiles. The device has a vertical resolution of 25 m in the 0–0.5 km range, 50 m in the 0.5–2 km range, and 250 m in the 2–10 km range. It should be noted that the vertical resolution reported here refers to the retrieval grid used for constructing the temperature and humidity profiles, rather than the intrinsic physical resolution of the microwave radiometer itself. The effective vertical resolution is mainly constrained by the information content of the observed microwave channels and the corresponding weighting functions. As a result, the number of independent pieces of vertical information (degrees of freedom for signal) is comparatively low, and the retrieved profiles represent smoothed atmospheric structures rather than fine-scale vertical details. Its maximum detection distance is 10 km. The QFW-6000 Microwave Radiometer features integrated temperature, humidity, and pressure sensors that provide real-time surface thermodynamic data for in-situ calibration and retrieval correction. Additionally, it incorporates a rain intensity sensor and an infrared cloud sensor to facilitate weather identification during rainy and cloudy conditions. The physical appearance of the QFW-6000 microwave radiometer is shown in Fig. 1.

批注 [滴滴14]: Thank you for this comment. In the revised manuscript (Page 3, Line 82-83), "flexible buoy monitoring platforms" has been replaced with "autonomous, multi-parameter buoy monitoring platforms".
(RC1, Line 70)

批注 [滴滴15]: Thank you for this comment. In the revised manuscript (Page 4, Line 99), we added references to support the description of the QFW-6000 microwave radiometer, including an official technical document and a peer-reviewed publication.
(RC1, Line 85)

批注 [滴滴16]: Thank you for this comment. In the revised manuscript (Page 4, Lines 102–103), we revised the wording to clarify that the V-band channels are used for temperature retrieval based on oxygen absorption, assuming a constant oxygen mixing ratio, rather than for direct oxygen detection.
(RC1, Line 90)

批注 [滴滴17]: Thank you for this suggestion. In the revised manuscript (Section 2.1, Pages 4, Lines 104–109), we clarified that the reported vertical resolution refers to the retrieval grid used to represent the temperature and humidity profiles, rather than an intrinsic measurement resolution of the radiometer. We also added a short explanation that the effective vertical resolution is limited by channel information content and weighting functions, and that the degrees of freedom for signal are comparatively low.
(RC2, Line 90)

Figure 1: The QFW-6000 microwave radiometric profiler developed by the CETC No.22 Research Institute was deployed for the experiment. The instrument features a K-band and V-band receiver for profiling tropospheric temperature and humidity.

The QFW-6000 microwave radiometric profiler belongs to the class of ground-based multi-channel microwave radiometers that have been widely used for atmospheric profiling. When properly calibrated, ground-based microwave radiometric profilers can provide brightness temperature measurements with absolute uncertainties on the order of a few tenths of a kelvin (e.g., Hewison, 2007; Cimini et al., 2006). The corresponding uncertainties in retrieved temperature profiles are generally on the order of 1–2 K in the lower troposphere, while relative humidity uncertainties are typically within 10–20 %, depending on atmospheric conditions and retrieval configuration. These ranges represent typical performance reported for this instrument class under proper calibration and favorable conditions, and may vary with calibration strategy and atmospheric conditions.

批注 [清清18]: Thank you for this comment. In the revised manuscript (Section 2.1, Page 5, Lines 116–122), we added typical uncertainty ranges for ground-based microwave radiometric profilers and included relevant references. The added text summarizes typical brightness temperature uncertainties (on the order of a few tenths of a kelvin) and typical retrieval uncertainties (about 1–2 K for temperature and about 10–20% for relative humidity, depending on conditions and configuration).
(RC2, Section 2.1, Line375)

2.2 The Buoy Platform

The buoy platform was developed by the Institute of Oceanographic Instrumentation, Shandong Academy of Sciences. The buoy has a UFO or disc-shaped appearance. It is constructed from a highly durable and corrosion-resistant, fully sealed, welded steel structure. The buoy body is 10 m in diameter and weighs approximately 30 tons. After modification, the platform can stably accommodate key equipment, such as the QFW-6000 microwave radiometer and attitude sensors. This adaptation to the marine environment ensures reliable data collection. The buoy's middle section houses a battery and an instrument compartment. Its exterior is composed of six buoyancy chambers to ensure stability and safety. The overall structural configuration of the buoy platform is illustrated in Fig. 2.

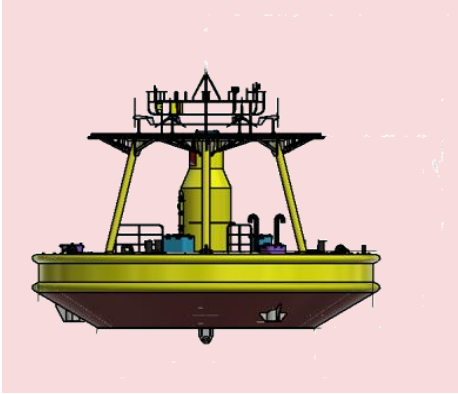

Figure 2: Structural design of the floating buoy platform independently developed by the Institute of Oceanographic Instrumentation, Shandong Academy of Sciences. The platform is equipped with the QFW-6000 microwave radiometer and attitude sensors and is designed for long-term stable operation in marine environments.

批注 [滴滴19]: Thank you for this suggestion. In the revised manuscript (Section 2.2, Page 5, Line 131), we added a schematic illustration of the buoy platform (Fig. 2).
(RC1, Line 101)

2.3 Attitude Sensor

The attitude of the buoy is a key parameter affecting the measurement accuracy of microwave radiometers during maritime navigation. Attitude sensors are used to measure the roll angles and pitch angles of the measurement platform. The zenith angle θ can be obtained by substituting the attitude sensor output data into the derived calculation formula for the buoy attitude and zenith angles. The calculation formula for the buoy's zenith angle is as follows eq. (1):

$$\cos\theta = \cos\alpha\cos\beta \,, \tag{1}$$

By substituting this observed zenith angle into the atmospheric radiation transfer equation, the oblique path brightness temperature can be obtained. This enables attitude compensation and correction~~, which in turn improves retrieval accuracy.~~ by explicitly introducing the effective zenith angle into the radiative transfer forward model. The effective viewing geometry is computed from real-time pitch and roll measurements and applied before inversion, thereby removing systematic brightness temperature deviations induced by platform motion. A MEMS-based attitude sensor integrating a tri-axis accelerometer, gyroscope, and digital motion processor (DMP) is used, with a typical static accuracy of 0.1°–0.3° and a dynamic accuracy of 0.3°–0.5° under typical marine operating conditions. A dedicated pointing alignment calibration was performed before deployment to ensure that the radiometer antenna corresponds to a zenith angle of 0° when the buoy is horizontally leveled.

批注 [滴滴20]: Thank you for this correction. In the revised manuscript (Page 6, Line 141), the term "microwave radiation equation" has been replaced with "atmospheric radiative transfer equation".
(RC1, Line 112)

批注 [滴滴21]: Thank you for this comment. In the revised manuscript (Page 6, Lines 142–148), we added a description of the zenith-angle correction procedure, the attitude sensor accuracy, and the antenna pointing-alignment calibration. Specifically, real-time pitch and roll measurements are used to compute the effective zenith angle, which is incorporated into the forward radiative transfer model to correct brightness temperature deviations caused by platform motion. We also added the attitude sensor accuracy (static: 0.1°–0.3°, dynamic: 0.3°–0.5°) and clarified that a pointing-alignment calibration was performed before deployment to ensure that the antenna corresponds to a zenith angle of 0° when the buoy is horizontally leveled.
(RC1, Line 113)

2.4 The Sites

The Jiaozhou Bay area off the coast of Qingdao (36.0721540° N, 120.3047530° E) was used as the sea trial research area. As shown in Fig.3, the retrieval data of microwave radiometer atmospheric temperature and humidity profiles were systematically

analyzed. For comparative analysis and validation, radiosonde data from the Qingdao Observatory (Station ID: 54857; 36.0702040° N, 120.3331640° E) in the upper-air sounding database of the University of Wyoming, USA, were selected (http://weather.uwyo.edu/upperair/bufrraob.shtml). The two sites are 2.5 km apart. Therefore, the microwave radiometer data and the radio sounding data can be considered co-located observation data. The sea trial experimental environment is shown in Fig.4.

Figure 3: Map of the Jiaozhou Gulf region showing the experimental sites. The red triangle indicates the location of the Buoy-based Microwave Radiometer (36.0721540° N, 120.3047530° E), and the yellow circle represents the Radiosonde Station (36.0702040° N, 120.3331640° E). The two instruments are separated by a distance of approximately 2.5 km. Basemap from Cartopy Quadtree Tiles.

Figure 4: Schematic of the sea trial experimental setup on the 10-meter diameter buoy platform. Key components include: the attitude sensor (top left) for monitoring platform roll and pitch; the QFW-6000 atmospheric brightness temperature measurement unit (bottom left) installed on the upper deck; and the OceanBuoy Host (right) for data aggregation and transmission. The red circles in the central photograph indicate the mounting positions of the sensors on the buoy structure.

In the Jiaozhou Bay area~~, the modified and liquid nitrogen-calibrated QFW-6000 microwave radiometer and attitude sensor will be attached to a 10-meter buoy platform according to the layout shown in Fig.3~~ the QFW-6000 microwave radiometer, which was modified and calibrated with liquid nitrogen on land before deployment, along with an attitude sensor, will be installed on a 10-meter buoy platform according to the layout shown in Fig.4. Brightness temperature and tilt angle will be collected simultaneously at the buoy's top level. Data will be aggregated via the serial port to the OceanBuoy Host. After data retrieval is completed, results will be transmitted back to the shore station.

批注 [清清22]: Thank you for this comment. In the revised manuscript (Page 7, Lines 166–168), we clarified that the liquid nitrogen calibration of the QFW-6000 microwave radiometer was performed on land prior to buoy deployment.
(RC1, Line 131)

3 Data, Model, and Method

To provide an intuitive overview of the proposed retrieval strategy, Fig. 5 illustrates the complete workflow of the buoy-based temperature and humidity profile retrieval. The procedure consists of four main parts: (1) preprocessing and attitude correction of microwave radiometer observations, (2) construction of the forward radiative transfer model and objective functions, (3) multi-objective optimization using the NSGA-II algorithm with physical constraints, and (4) systematic error correction and final profile generation.

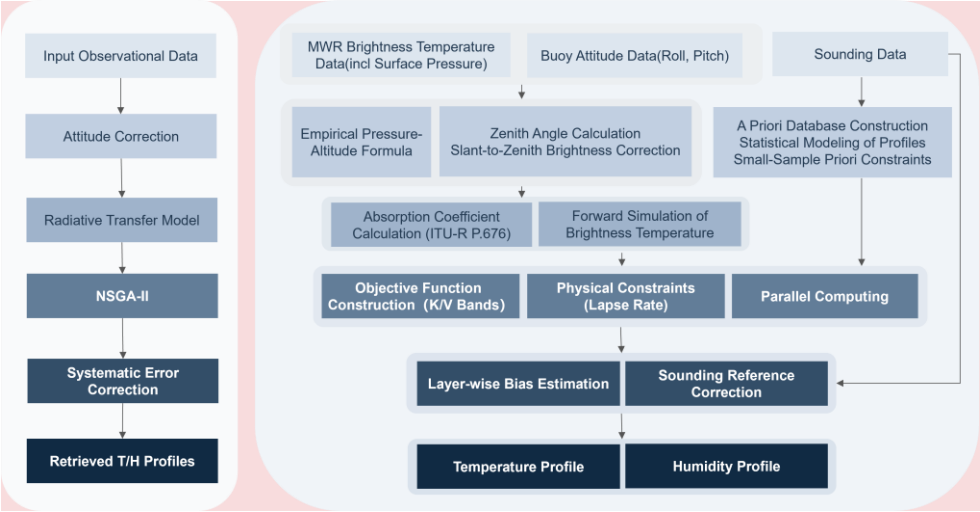

Figure 5. Schematic flowchart of the atmospheric temperature and humidity profile inversion method based on a microwave radiometer on a buoy platform. The workflow includes attitude correction of microwave radiometer observations, radiative transfer modeling and brightness temperature simulation, construction of multi-objective functions with physical constraints, NSGA-II optimization, and systematic error correction, resulting in the final retrieved temperature and humidity profiles.

3.1 The Data Source

Observed brightness temperature data were derived from the QFW-6000 microwave radiometer. The sounding data are from the University of Wyoming sounding station database. According to Tu et al. (2021), the Qingdao upper-air sounding system (Station ID: 54857) is based on the GTS1 radiosonde. According to the manufacturer's technical specifications, the GTS1 radiosonde provides continuous vertical profiles with a typical vertical resolution of approximately 5–10 m during ascent. The measurement accuracies are approximately ±0.2 K for temperature, ±5% for relative humidity, and ±1 hPa for pressure. Specifically, data from the Qingdao Meteorological Observatory (Station ID:54857) are used. The data are collected twice daily at 00:00 and 12:00 UTC. Attitude data are obtained from the attitude sensor in the buoy platform. The sensor collects attitude data every second. The zenith angle data are derived using the buoy attitude angle and the zenith angle calculation formula. Using the microwave radiation transfer equation, brightness temperature data along the inclined path can be corrected to that of the zenith path.

批注 [滴滴23]: Thank you for this suggestion. In the revised manuscript, we added a schematic flowchart at the beginning of Section 3 (pages 7-8, lines 172–181; new Fig. 5). The figure provides an overview of the main processing steps, including input data, correction procedures, forward modelling, NSGA-II optimization, and profile generation.
(RC2, Section 3)

批注 [滴滴24]: Thank you for this comment. In the revised manuscript (Page 8, Lines 184–187), we added the radiosonde instrument information for the University of Wyoming sounding data, including the instrument model, vertical resolution, and measurement accuracy. Specifically, we clarified that the observations are based on the GTS1 radiosonde, with a typical vertical resolution of approximately 5–10 m and measurement accuracies of ±0.2 K (temperature), ±5% (relative humidity), and ±1 hPa (pressure).
(RC1, Line 137)

3.2 Atmospheric Radiative Transfer Principle and Model

This section describes the forward radiative transfer modelling framework used in this study, including the calculation of atmospheric absorption coefficients and the corresponding microwave radiative transfer formulation. Ground-based microwave radiometry retrieves atmospheric profiles by measuring the downwelling thermal emission from the atmosphere. Under the Rayleigh-Jeans approximation, which is valid for microwave frequencies (300 MHz – 300 GHz), the brightness temperature (T_B) observed by a zenith-viewing radiometer can be expressed by the radiative transfer equation (RTE):

$$T = T_\infty \exp(-\int_0^\infty k_a \sec\theta dz) + \int_0^\infty T(z) k_a \exp\left(-\int_0^z k_a \sec\theta dz\right) \sec\theta dz, \quad (2)$$

where T_∞ is the cosmic background brightness temperature (approx. 2.73 K), $T(z)$ is the atmospheric physical temperature at altitude z, an $\tau(0,\infty)$ is the total optical depth. The term $k_\alpha(z)$ represents the atmospheric absorption coefficient at altitude z, which is the summation of contributions from oxygen, water vapor, and liquid water.

Accurate calculation of k_α is critical for the forward model. In this study, we selected the ITU-R P.676-13 model (ITU-R, 2022) to calculate these absorption coefficients. Compared to the MPM series and MonoRTM models mentioned above, the ITU-R model is recognised as the international standard for radio propagation engineering. It utilises a line-by-line summation method that offers an optimal balance between computational efficiency and accuracy, making it particularly suitable for the real-time retrieval requirements of this buoy-based system. This model uses a parameterized line-by-line summation formulation to compute the absorption lines of atmospheric gases. Specifically, the K-band channels (22-31 GHz) operate near the water vapor absorption line (22.235 GHz) to retrieve humidity information, while the V-band channels (51-58 GHz) operate along the oxygen absorption complex to retrieve temperature profiles (Philip, 1998). Liquid water scattering is neglected since absorption dominates over scattering in non-precipitating clouds within these frequency bands.

3.3 The Retrieval Algorithm Construction

To provide a unified and reproducible description of the retrieval framework, the temperature–humidity profile inversion is formulated as a constrained multi-objective optimization problem and solved using the Non-dominated Sorting Genetic Algorithm II (NSGA-II).

The retrieval aims to simultaneously minimize the residuals between simulated and observed brightness temperatures of temperature-sensitive (V-band) and humidity-sensitive (K-band) channels under physical consistency constraints derived from atmospheric lapse rate characteristics. The forward model is based on the atmospheric microwave radiative transfer equation and the ITU-R P.676-13 absorption model.

批注 [滴滴25]: Thank you for this important comment. In the revised manuscript (Page 9, Lines 204–207), we added the formal reference to the ITU-R gaseous absorption model (ITU-R Recommendation P.676-13, ITU-R, 2022) and expanded the explanation for selecting this model. Specifically, we clarified that while the MPM-series and MonoRTM models are based on detailed molecular spectroscopy, the ITU-R model provides fully documented parametric formulations with publicly available coefficients and offers a good balance between computational efficiency and modelling accuracy, making it suitable for real-time forward modelling and retrieval in buoy-based microwave radiometer applications.
(RC1, Line 147)

批注 [滴滴26]: Thank you for this comment. In the revised manuscript (Page 9, Lines 193–211), we merged the original Sections 3.2 and 3.3 into a single subsection and reorganized the content. The revised subsection is now entitled "Atmospheric Radiative Transfer Principle and Model" and provides a unified description of the forward modelling framework, including the calculation of atmospheric absorption coefficients using the ITU-R P.676-13 model and the forward simulation of brightness temperatures using the radiative transfer equation. In addition, we removed unnecessary background descriptions (e.g., wave–particle duality) and corrected the definition of the microwave frequency range to be consistent with standard microwave remote sensing literature.
(RC1, Line 157)

The optimization problem is solved through Pareto-front evolution using NSGA-II. To meet the real-time requirements of marine applications, a parallel computing strategy is introduced to accelerate population evaluation while keeping the mathematical formulation unchanged. The final retrieval profile is selected from the Pareto-optimal solution set using a joint error minimization criterion.

3.3.1 Data Preprocessing

This study conducted a comprehensive statistical analysis of the routine radiosonde data. We aimed to accurately obtain the ~~normal distribution patterns~~ statistical distribution characteristics of temperature and humidity. Based on the ~~theory of normal distribution confidence intervals, abnormal-sounding data deviating from the normal range were excluded~~ statistical analysis, data points falling outside the confidence interval(defined as the $\mu \pm 2$ standard deviations) were identified as outliers and excluded. Theory of normal distribution confidence intervals, abnormal-sounding data deviating from the normal range were excluded. ~~Additionally, radiosonde data are influenced by factors such as ascent speed and wind. This leads to inconsistent measurement data at different altitudes. To address these data-mismatch issues, linear interpolation was performed on the collected radiosonde data.~~ Additionally, radiosonde measurements are influenced by ascent rate and horizontal drift caused by wind, leading to irregular vertical sampling intervals. To address these grid mismatch issues, linear-interpolation was performed on the collected radiosonde data.

Furthermore, pressure profiles were obtained using actual ground-based pressure sensor data combined with empirical pressure-altitude formulas. To obtain pressure profiles for the specific experimental region, we adopted a hybrid empirical approach that combines local statistical climatology with standard engineering modeling. The pressure P (kPa) at a given altitude H (m) is calculated as the arithmetic mean of two components eq.(3):

$$P(H) = 0.5 \times P_{local}(H) + 0.5 \times P_{std}(H) \quad (3)$$

Where:

$P_{local}(H)$ represents the regional statistical fit, derived from a polynomial regression of historical pressure-altitude data from major cities in China:

$$P_{local} = 101.3 \times (5.3788 \times 10^{-9} H^2 - 1.1975 \times 10^{-4} H + 1) \quad (4)$$

$P_{std}(H)$ represents the standard atmospheric model defined in the national electric power industry code DL/T 5240-2010(National Energy Administration):

$$P_{std} = 101.3 \times \left[1 - 0.0255 \times \frac{H}{1000}\left(\frac{6357}{6357+\frac{H}{1000}}\right)\right]^{5.256} \quad (5)$$

This weighted combination effectively mitigates the systematic bias of the general standard model while retaining the physical consistency required for vertical profiling.

批注 [滴滴27]: Thank you for this important clarification. In the revised manuscript (Page 10, Lines 226–227), we explicitly defined the "normal range" as the confidence interval given by the mean ± 2 standard deviations (μ ± 2σ). Data points outside this interval are treated as outliers and excluded from subsequent analysis.
(RC1, Line 189)

批注 [滴滴28]: Thank you for this important clarification. In the revised manuscript (Page 10, Lines 225–226), we revised the wording to avoid implying a normal distribution assumption. The original expression "normal distribution patterns" has been replaced with "statistical distribution characteristics of temperature and humidity". We now clarify that normality is not assumed for the atmospheric variables themselves, but is only used as a statistical criterion for data quality control and outlier detection.
(RC1, Line 188)

批注 [滴滴29]: We thank the reviewer for this helpful clarification. In the revised manuscript (Page 10, Lines 228–230), we replaced the ambiguous wording "inconsistent measurement data at different altitudes" with "irregular vertical sampling intervals". This clarifies that the statement refers to non-uniform vertical sampling caused by variations in balloon ascent rate and wind-induced drift, rather than implying any physical discontinuity in the radiosonde profile.
(RC1, Line 190)

批注 [滴滴30]: We thank the reviewer for this careful comment. In the revised manuscript, we clarified that the "pressure–altitude model" refers to an empirical pressure–altitude equation. Specifically, in the Abstract (Page 1, Line 20), the wording has been revised from "pressure–altitude model" to "empirical pressure–altitude equation". In addition, in Section 3.3.1 (Page 10, Lines 231–244), we revised Eq. (3) and described it as a weighted combination of a regional empirical polynomial fit derived from historical pressure–altitude statistics and the standard atmospheric pressure model defined in DL/T 5240–2010.
(RC1, Line 18)

3.3.2 Construction of Atmospheric Prior Experience Database

It should be emphasized that only a limited amount of local radiosonde data is required to construct the small-sample prior experience database, which serves solely as an initial physical constraint for the retrieval process. During subsequent online retrieval, no historical data input is required. The preprocessed radiosonde data were interpolated to the same 83 height levels as the microwave radiometer using linear interpolation. A monthly statistical analysis revealed that temperature and humidity (T, H) at each height layer conformed to a normal distribution. The variables were substituted into the formulas $N\left(\mu_i^T, \sigma_i^T\right)$ and $N\left(\mu_i^{\mathrm{H}}, \sigma_i^{\mathrm{H}}\right)$. ~~It was found that atmospheric temperature followed a perfect normal distribution, while relative humidity exhibited a skewed distribution. The skewed variables were then transformed by taking their natural logarithms. They were then fitted to a normal distribution. Within the interval $\left[\mu_i^T - 2\sigma_i^T, \mu_i^T + 2\sigma_i^T\right]$, the sounding data values were set to $\begin{cases} T_i^{\min} = \mu_i^T - 2\sigma_i^T, T_i^{\max} = \mu_i^T + 2\sigma_i^T \\ H_i^{\min} = \mu_i^H - 2\sigma_i^H, H_i^{\max} = \max(H_i) \end{cases}$~~. To quantitatively assess the normality of the data distribution, we performed a monthly statistical analysis of temperature (T) and relative humidity (H) at each height layer. We calculated the Skewness (S) and Excess Kurtosis (K) for both variables. A distribution is considered to be approximately normal when $|S| < 1$ and $|K| < 1$ (Kim, 2013).

Taking the 50 m height layer in January as an example (Figure 6), the atmospheric temperature exhibits a high degree of symmetry with $S = -0.58$ and $K = 0.82$, indicating a good fit with the normal distribution. Similarly, the relative humidity at this level also demonstrates approximate normality ($S = -0.14$, $K = -0.70$). Based on these statistical characteristics, we constructed the empirical database by filtering out outliers falling outside the $\left[\mu_i^T - 2\sigma_i^T, \mu_i^T + 2\sigma_i^T\right]$ interval to ensure strict data quality. Specifically, values exceeding the boundaries were truncated to the threshold limits: $\begin{cases} T_i^{\min} = \mu_i^T - 2\sigma_i^T, T_i^{\max} = \mu_i^T + 2\sigma_i^T \\ H_i^{\min} = \mu_i^H - 2\sigma_i^H, H_i^{\max} = \max(H_i) \end{cases}$.This rigorous screening process effectively eliminated anomalous sounding data and finalized the construction of the empirical database.

批注 [滴滴31]: Thank you for this comment. In the revised manuscript, we clarified the role of radiosonde data in both the Abstract (Page 1, Lines 17–20) and Section 3.3.2 (Page 11, Lines 246–248). We clarified that only a limited amount of local radiosonde data is used to construct the prior database, and that no historical data input is required during the subsequent online retrieval stage.
(RC1, Line 16)

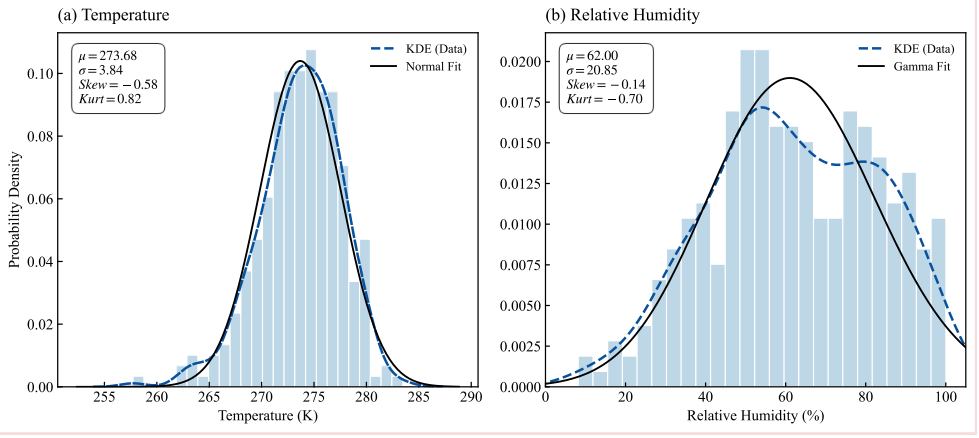

Figure 6. Probability density distributions of (a) temperature and (b) relative humidity at 50 m height in January. The black solid line represents the fitted normal distribution curve, and the blue dashed line represents the kernel density estimation (KDE). Statistical metrics (μ, σ, S, K) are annotated.

3.3.3 NSGA-II

To clarify how the retrieval is actually performed, the complete inversion workflow is illustrated in Fig. 4. Based on this framework, the retrieval procedure consists of the following main steps: construction of the objective functions from brightness temperature observations, introduction of physical constraints, multi-objective optimization using the NSGA-II algorithm, and subsequent systematic error correction to obtain the final temperature and humidity profiles. Addressing the challenges of sparse data, significant dynamic platform disturbances, and the high computational cost of traditional inversion methods requiring large training ~~samples~~ datasets in ocean observations, this study builds upon the NSGA-II (Deb et al., 2002) framework. It should be clarified that the proposed retrieval method is not based on the Optimal Estimation Method (OEM), but is formulated as a constrained multi-objective optimization problem solved using NSGA-II.~~Addressing the challenges of sparse data, significant dynamic platform disturbances, and the high computational cost of traditional inversion methods requiring large samples datasets in ocean observations, this study builds upon the NOGA-II framework.~~

~~It implements essential enhancements in three key areas: small-sample constraints, embedded physical laws, and dynamic attitude compensation. Supplemented by parallel computing and systematic error correction, the approach adapts to real-world scenarios characterized by sparse ocean observation data and unstable platforms. For the first time, it achieves high-precision temperature and humidity profile inversion under small-sample conditions and dynamic ocean environments. Specifically: (1) A small-sample prior knowledge base is constructed, significantly reducing reliance on massive training data through statistical modeling and physical boundary constraints; (2) Physical laws such as atmospheric lapse rates are introduced as hard constraints, effectively suppressing inversion results that violate physical principles; (3) Integrated attitude sensor data to~~

批注 [滴滴32]: We thank the reviewer for this constructive and valuable suggestion. In the revised manuscript (Page 11, Lines 251–264), we revised the statistical analysis description. Specifically, we removed the imprecise wording “perfect normal distribution” and replaced it with “approximate normal distribution”. We introduced Skewness (S) and Excess Kurtosis (K) as quantitative indicators to assess distribution normality and adopted the criteria |S| < 1 and |K| < 1 following Kim (2013). In addition, we added a new figure (Fig. 5) showing the probability density distributions of temperature and relative humidity at a representative height level together with fitted normal distributions for comparison.
(RC1, Line 196)

批注 [滴滴33]: Thank you for pointing this out. In the revised manuscript, we added a retrieval workflow flowchart at the beginning of Section 3 (new Fig. 5). We also added a short step-by-step description of the retrieval procedure in Section 3.3.3 (Page 10, Lines 267–270).
(RC2, Line 219)

批注 [滴滴34]: Thank you for this comment. In the revised manuscript, we clarified the role of radiosonde data in both the Abstract (Page 1, Lines 17–20) and Section 3.3.2 (Page 11, Lines 246–248). We clarified that only a limited amount of local radiosonde data is used to construct the prior database, and that no historical data input is required during the subsequent online retrieval stage.
(RC1, Line 16)

批注 [滴滴35]: We thank the reviewer for this important comment. In the revised manuscript, we corrected the typographical error by replacing “NOGA-II” with “NSGA-II” throughout the text. In addition, we added the original reference for the NSGA-II algorithm (Deb et al., 2002) in the revised manuscript (Page 12, Line 271).
(RC1, Line 204)

批注 [滴滴36]: Thank you for this question. The retrieval method used in this study is not based on optimal estimation (OEM). In the revised manuscript (Page 12, Lines 269–273), we clarified that the retrieval is formulated as a physically constrained multi-objective optimization problem and solved using the NSGA-II algorithm. We also corrected the typographical error “NOGA-II” to “NSGA-II” throughout the manuscript and added the standard reference for NSGA-II (Deb et al., 2002).
(RC2, Line 221)

~~compensate in real-time for zenith angle deviations caused by platform sway, enhancing robustness in dynamic conditions. Furthermore, employing a parallel computing architecture and systematic error correction mechanism, the single-run inversion time was reduced to the second level under parameter configurations of 175 individuals, 10 generations, a crossover probability of 0.9, and a mutation probability of 0.2, meeting the requirements for real-time maritime applications. The specific inversion workflow is designed as follows:~~

Specifically, a small-sample prior knowledge base is constructed to reduce dependence on large training datasets through statistical boundary generation and physical boundary constraints, as described in Section 3.3.2. Physical laws, including atmospheric thermodynamic lapse-rate constraints and physically admissible temperature–humidity bounds, are introduced as hard constraints to suppress inversion results that violate physical principles.

In addition, real-time attitude sensor measurements are integrated to compensate for zenith-angle deviations caused by platform motion. The effective viewing geometry is computed from real-time pitch and roll measurements and applied in the radiative transfer forward model before inversion, as detailed in Section 2.3.

Furthermore, by employing a parallel computing architecture and a systematic error correction mechanism, the single-run inversion time is typically below 1 min under a parameter configuration of 175 individuals and 10 generations (with a crossover probability of 0.9 and a mutation probability of 0.2) on a multi-core CPU. This computational cost is acceptable for operational shipborne applications and enables quasi-real-time processing of the observed data.

In operational marine meteorology and nowcasting, real-time processing typically refers to observational data being processed and delivered within minutes in order to support rapid update cycles for monitoring and decision support. According to the WMO Guide to Meteorological Instruments and Methods of Observation (WMO, 2018), operational observing systems commonly operate with reporting intervals on the order of 1–10 minutes. In addition, Sun et al. (2014) indicate that convective nowcasting systems require update cycles of approximately 5–10 minutes to capture fast-evolving atmospheric states.

In this context, the proposed framework achieves a single-run inversion time within ~1 min, which is well within the typical reporting and update intervals required for operational maritime monitoring and nowcasting.

The Level-1 data processing workflow, including brightness temperature quality control, temporal synchronization, and vertical interpolation, is described in Section 3.1. The complete inversion workflow is designed as follows:

1. Construction of the Objective Function

The core of the retrieval process is an established multi-objective optimization problem. The objective is to minimize the difference between simulated and measured brightness temperatures. Physical constraints are introduced to ensure the reasonableness of the retrieval results. Specifically, the objective function $\begin{cases} min \left| \tilde{T}_{ret}^{22\mathrm{GHz}} - T_{obs}^{22\mathrm{GHz}} \right| \\ min \left| \tilde{T}_{ret}^{58\mathrm{GHz}} - T_{obs}^{58\mathrm{GHz}} \right| \end{cases}$ is constructed based on the difference between simulated and measured brightness temperatures from microwave radiometers in the K/V bands. Specifically, the objective function is constructed from the residuals between simulated and observed brightness temperatures in the K-band (22 GHz) and V-band (58 GHz). In this formulation, $\tilde{T}_{ret}$ and T_{obs} denote the simulated and measured brightness temperatures, respectively, and the superscripts indicate the corresponding frequency channels. ~~Here, $\tilde{T}_{ret}^{22\mathrm{GHz}}$ denotes the~~

批注 [滴滴37]: Thank you for this comment. In the revised manuscript (Page 12, Lines 281–284), we clarified that *single-run inversion time* denotes the wall-clock time for one retrieval under the specified NSGA-II configuration and multi-core parallel execution. We also compared the resulting runtime (~1 min) with typical operational reporting/update intervals (WMO, 2018; Sun et al., 2014), showing that the computational cost supports quasi-real-time processing.
(RC2, Line 216)

批注 [滴滴38]: We thank the reviewer for these constructive comments. In the revised manuscript (Page 12–13, Lines 273–293), we revised Section 3.3.3 to remove imprecise wording and overstated performance descriptions, and added a clearer step-by-step description of the retrieval workflow, including Level-1 data processing, physical constraints, and attitude data fusion. In addition, we clarified the definition of real-time maritime applications and added relevant operational references (WMO, 2018; Sun et al., 2014).
(RC1, Lines 207, 209, 210, 216)

~~simulated brightness temperature in the microwave radiometer's K-band, T_{obs}^{22GHz} represents the measured brightness temperature in the K-band channel, T_{cal}^{58GHz} indicates the simulated brightness temperature in the V-band, T_{obs}^{58GHz} denotes the measured brightness temperature of the microwave radiometer's V-band channel.~~ Additionally, atmospheric physical characteristics, such as temperature and humidity lapse rates(implemented as inter-layer difference constraints; applied to all adjacent layers) $\begin{cases} \min\limits_{i\in N, i\leqslant 83} |T_{i+1} - T_i| \leqslant \delta_1 \\ \min\limits_{i\in N, i\leqslant 83} |H_{i+1} - H_i| \leqslant \delta_2 \end{cases}$, are incorporated into the constraint system. Here, N denotes the maximum index of the vertical levels,~~value obtained for i,~~ δ_1 represents the maximum allowable humidity difference between adjacent levels. In practice, this constraint is applied to each pair of adjacent layers (i.e., $|T_{i+1} - T_i| \leq \delta_1$ and $|H_{i+1} - H_i| \leq \delta_2$ for all i), which serves as an inter-layer continuity (smoothness) constraint to limit excessive layer-to-layer variations. ~~temperature lapse rate, and δ_2 denotes the maximum humidity lapse rate. Given the general trend that temperature and humidity typically decrease with increasing altitude in the troposphere, these lapse rate trends are used as constraints.~~

It should be noted that this so-called "lapse rate constraint" does not enforce a monotonic decrease of temperature with height. Because it constrains the absolute value of the layer-to-layer difference, both positive and negative temperature gradients are allowed; therefore, temperature inversions are permitted as long as the local layer-to-layer changes remain within the prescribed bounds. This limits non-physical results that may arise during the retrieval process. By integrating these objectives and constraints,~~. t~~This transforms the retrieval problem into an optimization problem, which requires the solution of an optimal profile.

2. Initialization of the Population

First, reasonable value ranges are defined for the temperature and humidity variables at each altitude layer using the constructed atmospheric prior experience database. Within this probability boundary, an initial population is generated through random sampling. Each individual represents a complete set of potential temperature-humidity profile solutions. Next, the fitness of each individual in the population is assessed. To ensure population diversity and convergence, key techniques from the non-dominance sorting genetic algorithm (NSGA-II) are employed. To ensure both convergence and diversity of the solution set, Pareto dominance is used to rank individuals into different non-dominated fronts according to the multiple objective functions, while a density-based sorting strategy (crowding distance) is applied to maintain solution diversity along the Pareto front. This multi-objective selection mechanism allows the algorithm to search for stable atmospheric temperature and humidity profiles while avoiding premature convergence (Deb et al., 2002)~~These techniques, such as density sorting and Pareto dominance, are used to evaluate and select the offspring population.~~

3. Parallel Computing Optimization

We introduced parallel computing technology to optimize algorithm efficiency. Specifically, we used a controller-worker~~master-slave~~ parallel mode. This mode divides the population into multiple sub-populations, which are then assigned to different CPUs for independent calculations. The ~~master processor~~ controller processor manages task allocation and result

批注 [滴滴39]: Thank you for this suggestion. In the revised manuscript (Page 12-13, Lines 299–301), the paragraph has been shortened by removing repetitive descriptions and presenting the objective function in a unified formulation.
(RC2, Lines 223–226)

批注 [滴滴40]: Thank you for this question. In the revised manuscript (Section 3.4.3, Page 13, Lines 302–312), we clarified that the "lapse rate constraint" used here is implemented as an inter-layer continuity (smoothness) constraint that limits layer-to-layer differences, rather than enforcing a monotonic temperature decrease with height. Because the constraint is based on the absolute magnitude of adjacent-layer differences, temperature inversion structures are not suppressed as long as the gradients remain within the prescribed bounds.
(RC2, Section 3.4.3, Line 212)

批注 [滴滴41]: Thank you for this suggestion. In the revised manuscript (Page 13, Lines 317–322), we added a short description of Pareto dominance and density-based sorting (crowding distance) and included the standard NSGA-II reference (Deb et al., 2002).
(RC2, Paragraph 2)

aggregation, while the worker ~~The slave~~ processors complete their computation~~calculations~~ and return~~report~~ the results ~~back~~. This approach significantly improves the computational efficiency of the retrieval ~~efficiency~~process.

4. Obtaining the Optimal Solution

After the genetic algorithm completes its preset number of iterations, a set of multiple Pareto optimal solutions is produced. To select the final optimal solution from this set, a hybrid reconstruction strategy is employed. First, the extreme optimal values for each objective function are identified. These are the solutions in the Pareto optimal solution set that minimize the difference between the simulated and measured brightness temperatures in the K/V band. Subsequently, these solutions with extreme optimal values are mixed and reconstructed across different objectives. This generates a solution with the best overall performance. This solution serves as the final retrieval result.

5. System Error Correction

To further improve the accuracy of the retrieval results, a system error correction method is designed and introduced. ~~A dataset of 38 independent samples is randomly sampled. This is then divided into a training set (80 %) and a test set (20 %). The training set is used to establish the system error model. Meanwhile, the test set serves as an independent dataset to validate the effectiveness of the correction method. For temperature and humidity, the systematic error $E(h)$ at each height layer h is calculated as follows eq.(4) and eq.(5):~~ The 38 collocated samples were randomly divided into a training set (80%) and an independent testing set (20%). The training set was used to derive the systematic bias correction model, while the testing set was used exclusively for independent validation of the correction performance. For temperature and humidity, the systematic error $E(h)$ at each height layer h is calculated as follows eq.(6) and eq.(7):

$$E_T(h) = \frac{1}{M}\sum_{i=1}^{M}\left(T_{ret,i}(h) - T_{obs,i}(h)\right), \quad (6)$$

$$E_H(h) = \frac{1}{M}\sum_{i=1}^{M}\left(H_{ret,i}(h) - H_{obs,i}(h)\right), \quad (7)$$

Among these variables: $E_T(h)$ and $E_H(h)$ are the systematic errors in temperature and humidity at height h. M is the number of samples in the training set. $T_{ret,i}(h)$ and $H_{ret,i}(h)$ are the original retrieval values at height h for the i-th sample, while $T_{obs,i}(h)$ and $H_{obs,i}(h)$ are the corresponding sounding observation values. After the systematic error model is established using this method, it is applied to correct all retrieval profiles. The corrected temperature and humidity profiles, $T_{corr}(h)$ and $H_{corr}(h)$, are obtained by subtracting the corresponding systematic errors from the original retrieval profiles, $T_{ret}(h)$ and $H_{ret}(h)$. For temperature and humidity, the $T_{corr}(h)$ and $H_{corr}(h)$ calculated as follows eq.(8) and eq.(9):

$$T_{corr}(h) = T_{ret}(h) - E_T(h), \quad (8)$$

$$H_{corr}(h) = H_{ret}(h) - E_H(h), \quad (9)$$

The temperature and humidity profiles corrected for the system errors are the final retrieval results. It should be noted that the radiosonde observations are used only to estimate the height-dependent systematic error profile under land-based conditions

批注 [清清42]: Thank you for this suggestion. In the revised manuscript (Page 13, Lines 324–328), "master–slave" has been replaced with "controller–worker".
(RC2,Line241)

批注 [清清43]: We thank the reviewer for this important methodological question. In the revised manuscript (Section 3.3.3, Page 14, Lines 337–341), we clarified that the systematic bias correction model is not constructed using all available data. Instead, the collocated microwave radiometer–radiosonde observation pairs are randomly divided into a training set (80%) and an independent test set (20%). The training set is used to establish the bias correction model, while the statistical evaluation results and corrected retrieval profiles are derived from the independent test set.
(RC1, Line 258)

as part of an instrument calibration procedure. In operational applications over the open ocean, the derived systematic error profile can be applied as a fixed correction term and does not require the availability of concurrent radiosonde data.

To avoid overly optimistic performance estimates, the systematic error profile is derived from the training subset only, while the independent test subset is used exclusively for validation.

Specifically, Level-1 brightness temperature data are first calibrated and quality-controlled, followed by attitude-based geometric correction using real-time pitch and roll measurements. The effective zenith angle is computed and introduced into the radiative transfer forward model. A small-sample prior database is then constructed from historical radiosonde profiles using statistical boundary generation. Atmospheric thermodynamic lapse-rate constraints are introduced as hard physical constraints during optimization. The NSGA-II framework is subsequently employed to perform multi-objective inversion of temperature and humidity profiles under dynamic marine conditions.

批注 [滴滴44]: Clarification has been added to explain the role of radiosonde data in estimating the systematic error profile and to distinguish between the training subset used for error estimation and the independent test subset used for validation. (Page 14, Lines 352-357)
(RC2,Line253)

批注 [滴滴45]: we have expanded this section to describe the Level-1 brightness temperature processing in detail. Specifically, we now clarify how the real-time pitch and roll data from the attitude sensor are integrated with the forward radiative transfer model to perform geometric corrections and zenith angle computations.
(RC1,Line210)

4 Results

To comprehensively evaluate the performance and suitability of the proposed models for marine environments, microwave radiometer observation experiments were conducted on a buoy platform. This was done in the coastal waters of Jiaozhou Bay, Qingdao (36.0721540° N, 120.3047530° E). The models include the tropospheric temperature and humidity profile retrieval model and the buoy platform zenith compensation correction model. During the experiment, 38 sets of valid observational data were obtained. These data were compared with radio sounding data from the Qingdao Meteorological Observatory (Station ID: 54857) for validation. For each radiosonde launch time (00:00 and 12:00 UTC), the temporally co-located microwave radiometer retrieval record closest in time was selected for comparison. A matchup was considered valid only if the radiosonde profile passed quality control and was successfully interpolated onto the standard height grid of the microwave radiometer (0–10 km). This procedure ensures temporal consistency between the two observing systems and provides a reliable basis for profile-to-profile validation. The sounding data are from the Wyoming State University sounding database (36.0702040° N, 120.3331640° E). The two observation points are 2.5 km apart. Therefore, their data can be considered co-located observations. This provides reliable reference true values for model validation.

To quantitatively assess the performance of the proposed retrieval model, the retrieval accuracy is evaluated using the root mean square error (RMSE), which represents the statistical uncertainty of the retrieved profiles with respect to radiosonde observations. ~~To quantitatively assess the performance of the proposed retrieval model, the RMSE was calculated. The RMSE is the difference between the model retrieval results and the radiosonde data. RMSE serves as a standard metric for measuring the difference between model predictions and actual observations. The calculation formula is as follows eq.(10):~~

$$RMSE = \sqrt{\frac{1}{m}\sum_{i=1}^{m}(y^{i} - y)^{2}}, \quad (10)$$

~~In this equation, m represents the number of samples used in the calculation. y' represents the temperature and humidity profiles obtained through the model's retrieval. y represents the radio sounding observation data used as the true value for verification.~~

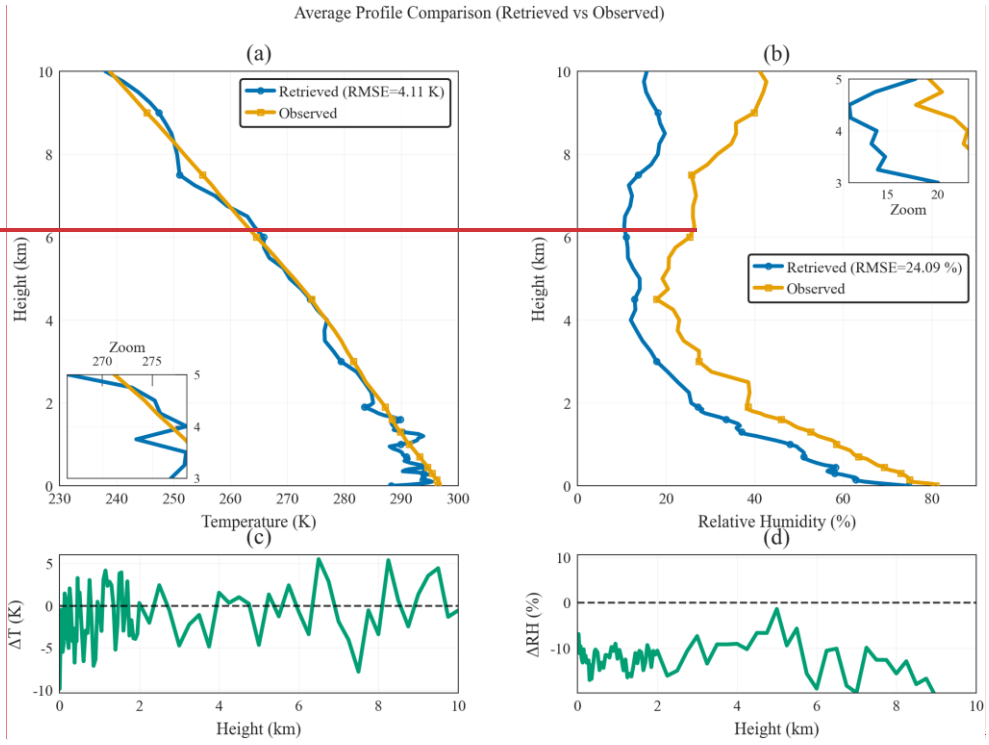

批注 [清清46]: Thank you for this suggestion. In the revised manuscript (Page 15, Lines 377-379), the RMSE formula and detailed definitions have been removed, and RMSE is now only mentioned as a statistical measure of retrieval uncertainty. **(RC2, Lines 278–282)**

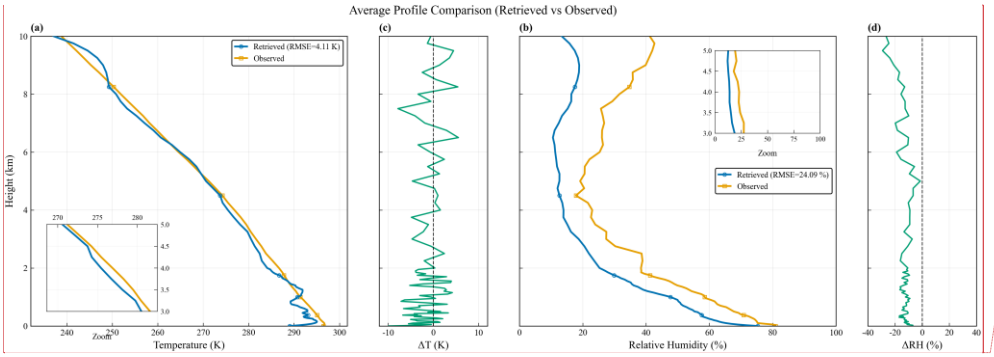

Figure 7: Statistical comparison of atmospheric profiles between the uncorrected NSGA-II retrievals and radiosonde observations. Panels (a) and (b) display the mean temperature and relative humidity profiles, respectively. The blue solid lines represent the initial retrievals from the buoy-based Microwave Radiometer (MWR) using the NSGA-II algorithm before systematic error correction, while the orange-yellow solid lines denote the co-located reference observations from the Qingdao Radiosonde Station (ID: 54857). Panels (c) and (d) illustrate the vertical distribution of the mean retrieval bias (Retrieved minus Observed) for temperature and humidity. The statistics are derived from the mean profiles of 38 valid matchups collected during the field campaign in Jiaozhou Bay from August 22 to September 23, 2023. The profiles are time-matched and interpolated onto a common vertical grid. The zoomed subplots use the same processed profiles with adjusted display ranges.

Figure 7 shows the average comparison between the temperature and humidity profiles retrieved by the NSGA-II algorithm without systematic error correction (blue solid lines) and the corresponding radiosonde observations from Jiaozhou Bay (orange-yellow solid lines), together with the vertical distribution of their differences. The profiles are time-matched and interpolated onto a common vertical grid within the effective vertical resolution of the radiometer. The main panels present the full-profile comparison, while the zoomed subplots display selected vertical ranges using the same processed profiles with adjusted display scales.

The radiosonde profiles shown here represent ensemble-averaged means over 38 matched cases, which suppress small-scale vertical variability and therefore appear smoother. In contrast, the retrieved profiles are obtained through layer-by-layer optimization on a discrete vertical grid, and weak layer-to-layer structures may remain, especially in altitude ranges where the sensitivity of the microwave weighting functions is reduced.

Figures 7(a) and 7(c) indicate that the retrieved temperature profiles show an overall agreement with the radiosonde observations in the near-surface layer (0–2 km), particularly in Fig. 7(c), where the deviations approach zero, demonstrating good retrieval performance in the lower troposphere. However, with increasing altitude, the temperature differences exhibit both positive and negative deviations in the middle troposphere (approximately 3–6 km). As shown in Fig. 7(c), the deviations generally remain within ±5 K, with larger fluctuations occurring around 4–5 km, which is consistent with the reduced sensitivity of the microwave channels at these heights. This altitude range corresponds to the trough region of the microwave

批注 [滴滴47]: Thank you for this suggestion. In the revised manuscript (Page 15, Line 380; Page 17, Line 416), panels (c) and (d) have been moved to the right of the corresponding profile panels so that all panels share the same vertical axis.
(RC2, Figures 4 and 5)

批注 [滴滴48]: Thank you for this comment. In the revised manuscript (Page 16, Line 399), "highly consistent" has been revised to "overall agreement". In addition, in Page 17-18, Line 431-432, "excellent accuracy" has been replaced with "good retrieval accuracy".
We also added typical uncertainty ranges for ground-based microwave radiometric profilers in Section 2.1 (Page 5, Lines 116–122), together with relevant references, to provide context for interpreting the observed deviations.
(RC2, Line 297)

批注 [滴滴49]: Thank you for this comment. In the revised manuscript (Page 16, Lines 401–404), the description has been revised to reflect the full range of deviations shown in the figure. The text now states that temperature differences in the 3–6 km layer generally remain within about ±5 K, consistent with the values shown in Fig. 7(c).
(RC2, Line 299)

weighting functions, where the retrieval sensitivity is reduced. Above approximately 6 km, the temperature differences show a reduced magnitude compared to the 3–6 km layer, although non-negligible fluctuations are still observed (Fig. 7(c)).

The relative humidity profiles (Figs. 7(b) and 7(d)) exhibit more complex deviation patterns. A positive bias of 5–15% occurs below 1–2 km, followed by a transition to a systematic negative bias of 10–25% between 2 and 5 km, peaking near 4 km. The liquid water path (LWP), provided as a standard Level-2 product of the QFW microwave radiometer, is used only as an auxiliary indicator for diagnosing cloud contamination and residual retrieval errors, rather than as an input variable to the inversion.

Overall, temperature errors are mainly concentrated between 3 and 6 km, while humidity errors cluster between 2 and 5 km. Although their peak altitudes overlap, their vertical structures differ significantly, indicating that the middle troposphere represents a relatively vulnerable layer for simultaneous temperature and humidity retrieval. These results suggest that localized systematic errors require further correction through height-dependent error modeling.

~~Figure 4 shows the average comparison between the temperature and humidity profiles (blue solid lines) retrieved by the NOGA-II algorithm without any systematic error correction and the true values from the Jiaozhou Bay radiosonde observations (orange-yellow solid lines), along with the distribution of their difference with height. Fig. 4(a) and 4(c) reveal that the temperature profile exhibits a trend highly consistent with the sounding data within the near-surface layer at 0–2 km, particularly in Fig. 4(c), where deviations approach the zero line, indicating good retrieval accuracy in the near-surface layer. However, with increasing altitude, the retrieval profile exhibits a systematic positive deviation of 1.5–3 K between 3 and 6 km, peaking at 4–5 km. This aligns precisely with the height at which sensitivity decreases in the trough region of the microwave 12-305-310-315 weighting function. Beyond 6 km, the deviation recedes to 1–2 K but persists as a weaker positive bias, indicating that while the upper-level accuracy improves, the systematic error remains unresolved. The deviation patterns in the relative humidity profiles (Fig.4(b) and 4(d)) are more complex: a positive deviation of 5–15% exists between 1–2 km, transitioning to a systematic negative deviation of 10–25% between 2–5 km, peaking near 4 km. This layer coincides with the sensitivity decline zone of the 22-GHz channel, where samples with cloud liquid water path greater than 0.2 mm exhibit the most significant residual influence. Above 5 km, the negative bias gradually converges but persists as a weaker 5–10% deviation, indicating vertical propagation of the mid-level dry bias. Overall, the uncorrected profile's systematic errors exhibit height-selective distribution in Fig.4(c) and (d). Temperature errors concentrate between 3–6 km, while humidity errors cluster between 2–5 km. Though their peak regions overlap, their shapes differ significantly. This further highlights the mesosphere as a "vulnerable zone" for simultaneous temperature-humidity retrieval, necessitating targeted correction through height-dependent error modeling. Overall, the uncorrected profiles capture the general distribution characteristics of tropospheric temperature and humidity. However, significant local systematic errors require further correction through error modeling. Therefore, this study incorporates systematic error correction processing.~~

批注 [清清50]: Thank you for this comment. In the revised manuscript (Page 16, Lines 405–406), the description has been revised to remove the unsupported quantitative claim ("1–2 K beyond 6 km") and to describe the trend shown in Fig. 4(c) in a qualitative and data-consistent manner.
RC2,Line301

批注 [清清51]: Thank you for pointing this out. In the revised manuscript (Page 16, Line 413), "mesosphere" has been corrected to "middle troposphere".
(RC2, Line 309)

批注 [清清52]: We thank the reviewer for these comments. In the revised manuscript (Page 15–16, Lines 387–415), we revised the text and figures to clarify the interpretation of the profile comparisons, ensure consistency between the main and zoomed panels, and correct the related terminology.
Specifically, we added a physical explanation for the apparent smoothness difference between radiosonde and retrieved profiles. The radiosonde profiles represent ensemble-averaged results from multiple collocated samples, while the radiometer retrieval profiles are obtained through discrete-layer inversion and may retain weak stratification structures depending on the weighting-function sensitivity.
We also unified the plotting workflow for the main panels and zoomed-in subpanels to ensure that the zoomed plots represent true magnifications of the corresponding sections in the main profiles without additional smoothing or processing.
In addition, we clarified the criteria for valid profile comparison, including temporal collocation, interpolation to a common vertical grid, and evaluation within the effective vertical resolution of the microwave radiometer.
We clarified that liquid water path (LWP) is not included as a state variable in the NSGA-II retrieval framework and is used only as an auxiliary diagnostic parameter for data quality control and error analysis. (Page 16, Lines 408-411)
Finally, we corrected the term "mesosphere" to "middle troposphere" to ensure consistency with the altitude range investigated in this study.(Page 16, Lines 413)
(RC1, Lines 286, 305, 309)

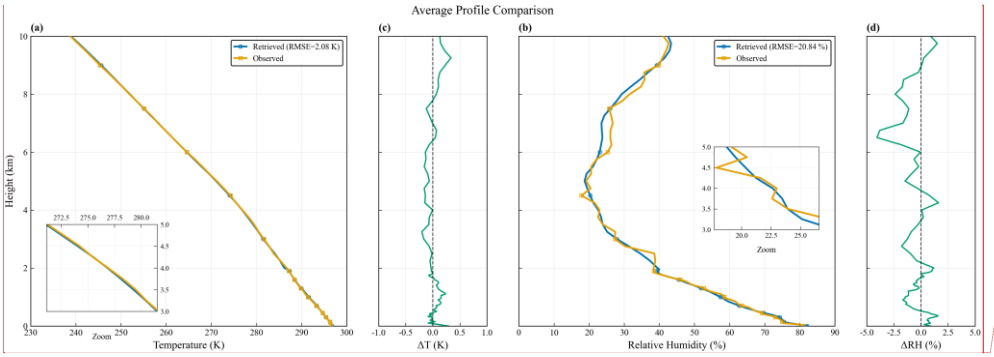

Figure 8: Comparison of retrieval results after applying the systematic error correction model. Panels (a) and (b) display the corrected temperature and relative humidity profiles, respectively. The blue solid lines represent the MWR retrieval results corrected by subtracting the systematic error profiles $E_T(h)$ and $E_H(h)$ as defined in Eqs. (6) and (7). The orange-yellow solid lines represent the reference radiosonde observations. Panels (c) and (d) display the residual error profiles after correction. Based on the 38 valid matchups, the Root Mean Square Error (RMSE) for the corrected profiles is reduced to 2.08 K for temperature and 20.95% for humidity across the 0–10 km vertical range. The corrected profiles shown in this figure are based on the independent testing subset and are not used in the construction of the bias correction model.

Figure 8 presents the comparison between the NSGA-II retrieved profiles (after systematic error correction) and the radiosonde observations. Compared to the pre-correction results, the retrieval accuracy has significantly improved. To further quantify the correction effectiveness and the overall retrieval performance, a detailed statistical summary of the 38 validation cases is provided in Table 1.

Table 1. Statistical summary of retrieval performance for temperature and humidity profiles across different altitude layers based on 38 validation cases.

Variable	Altitude Layer	MBE	RMSE	Correlation (R)
Temperature (K)	0-2 km	0.17	2.14	0.83
	2-10 km	0.30	2.34	0.99
	Overall (0-10 km)	**0.22**	**2.08**	**0.99**
Relative Humidity (%)	0-2 km	-1.71	18.79	0.57
	2-10 km	-0.17	25.25	0.27
	Overall (0-10 km)	**-1.12**	**20.95**	**0.66**

Temperature Retrieval Performance: As shown in Fig. 8(a) and Table 1, the corrected temperature retrieval demonstrates ~~excellent~~ good retrieval accuracy, with an overall correlation coefficient (R) of 0.99 and an RMSE of 2.08 K across the full vertical profile. The bias correction mainly removes the systematic (mean) component of the retrieval error, while random discrepancies caused by instrument noise and instantaneous atmospheric variability remain. The residual error profile in Fig. 8(c) confirms that the systematic bias has been largely eliminated (Overall MBE = 0.22 K). It is worth noting that while the

批注 [滴滴53]: Thank you for this suggestion. In the revised manuscript (Page 16, Line 375; Page 17, Line 411), panels (c) and (d) have been moved to the right of the corresponding profile panels so that all panels share the same vertical axis.
(RC2, Figures 4 and 5)

批注 [滴滴54]: Thank you for this comment. In the revised manuscript (Page 17, Lines 422–423 and 432–433), we clarified that the bias correction removes the height-dependent mean bias and is not intended to force point-by-point agreement between retrieved and radiosonde profiles. Small residual differences are therefore expected.
We also clarified that the bias correction model is trained using an independent calibration dataset and then applied to separate validation cases shown in the figure.
In addition, the plotting procedure has been unified so that the zoom panels are true magnifications of the corresponding parts of the main plot.
(RC1, Line 315)

批注 [滴滴55]: Thank you for this comment. In the revised manuscript (Page 16, Line 394), "highly consistent" has been revised to "overall agreement". In addition, in Page 18, Line 425, "excellent accuracy" has been replaced with "good retrieval accuracy".
We also added typical uncertainty ranges for ground-based microwave radiometric profilers in Section 2.1 (Page 5, Lines 117–123), together with relevant references, to provide context for interpreting the observed deviations.
(RC2, Line 297)

批注 [滴滴56]: Thank you for this comment. In the revised manuscript (Page 17, Lines 422–423 and 432–433), we clarified that the bias correction removes the height-dependent mean bias and is not intended to force point-by-point agreement between retrieved and radiosonde profiles. Small residual differences are therefore expected.
We also clarified that the bias correction model is trained using an independent calibration dataset and then applied to separate validation cases shown in the figure.
In addition, the plotting procedure has been unified so that the zoom panels are true magnifications of the corresponding parts of the main plot.
(RC1, Line 315)

correlation coefficient for the 0–2 km layer (R=0.83) is slightly lower than that of the 2–10 km layer (R=0.99), the RMSE indicates superior absolute accuracy in the near-surface layer (2.14 K vs. 2.34 K). The exceptionally high correlation in the 2–10 km range is largely driven by the significant temperature lapse rate across the troposphere, which dominates the statistical calculation. In contrast, the 0–2 km layer exhibits more complex thermal structures, which are inherently smoothed by the radiometric retrieval, leading to a slightly lower correlation despite the higher measurement precision.

Humidity Retrieval Performance: For relative humidity (Fig. 8(b)), the overall RMSE is 20.95% with a correlation of 0.66. As illustrated in Fig. 8(d) and quantified in Table 1, the systematic bias has been effectively minimized (Overall MBE = -1.12%). However, the correlation coefficients for humidity are lower compared to temperature (0.57 for 0–2 km and 0.27 for 2–10 km). This is attributed to three primary factors: (1) Vertical Resolution: Radiosondes capture high-frequency variations and sharp humidity gradients (e.g., cloud layers), whereas microwave radiometer retrievals are inherently smooth; (2) Spatial Mismatch: The high spatial variability of water vapor, combined with the 2.5 km separation between the buoy and the radiosonde station, introduces unavoidable discrepancies; and (3) Sensitivity Decay: In the middle and upper troposphere (2–10 km), the water vapor content is low, and the sensitivity of the K-band channels decreases, making the retrieval more susceptible to noise. Despite these physical limitations, the RMSE values indicate that the proposed method ~~provides value humidity information for marine monitoring.~~ provides operationally useful humidity information for routine marine environmental monitoring in data-sparse offshore regions. Consistent with previous studies using ground-based microwave radiometers, retrieval RMSE values on the order of 1–2 K for temperature and 10–30% for relative humidity are generally regarded as operationally useful (Massaro et al., 2015; Yan et al., 2020; Cimini et al., 2011). In summary, the sea trial results validate the effectiveness and feasibility of the proposed method. By constructing a small-scale prior experience database and integrating platform attitude information, the NSGA-II-based retrieval framework reduces the dependence on large historical training datasets. It should be noted that historical radiosonde observations are used only to characterize a height-dependent systematic bias profile, whereas the retrieval process itself does not rely on extensive historical training samples. The systematic bias profile is estimated from a training subset, and its correction performance is evaluated using an independent testing subset. The statistical results demonstrate that this approach provides a robust solution for real-time retrieval of tropospheric atmospheric parameters in data-sparse marine environments.~~the NSGA-II algorithm successfully overcomes reliance on extensive historical data. The statistical performance confirms that this approach provides a robust solution for real-time, stable retrieval of tropospheric atmospheric parameters in data-sparse marine environments~~

批注 [滴滴57]: Thank you for this comment. In the revised manuscript (Page 18, Line 446), we replaced "upper troposphere (2–10 km)" with "middle and upper troposphere (2–10 km)" to better reflect the typical vertical structure at these latitudes.
(RC1, Line 343)

批注 [滴滴58]: Revised this paragraph to clarify that the bias correction mainly removes the systematic (mean) component of the retrieval error, while random discrepancies caused by instrument noise and instantaneous atmospheric variability remain, explaining why the bias-corrected profiles do not fully coincide with the radiosonde observations. In addition, the altitude range is now described as the middle and upper troposphere (2–10 km) instead of the upper troposphere only, to ensure a physically accurate definition. Furthermore, representative RMSE ranges for marine monitoring are now specified and supported by previous studies, indicating what levels of accuracy are considered operationally useful (Referee #1, RC1 Lines 315, 343, and 345).

批注 [滴滴59]: Thank you for this comment. In the revised manuscript (Page 18, Lines 448–451), we added a short discussion of typical RMSE ranges reported for ground-based microwave radiometer retrievals and their typical application context. We clarified that temperature RMSE values of about 1–2 K and relative humidity RMSE values of about 10–30% are commonly considered suitable for routine operational monitoring. Relevant references have been added.
(RC1, Line 345)

批注 [滴滴60]: Thank you for this comment. In the revised manuscript (Page 18, Lines 453–458), we clarified that historical radiosonde data are used only to estimate a height-dependent systematic bias profile, rather than to train the retrieval algorithm itself. We also clarified that the bias profile is derived from a training subset and evaluated using an independent testing subset.
(RC2, Line 349)

5 Discussion

This study addresses the issues of sparse marine data and the reliance of traditional retrieval methods on large amounts of historical data. A method to retrieve tropospheric temperature and humidity profiles using a ground-based microwave radiometer is proposed and preliminarily validated. The method is based on a multi-objective genetic algorithm (NSGA-II). It has been successfully deployed on a buoy platform, thereby expanding the marine application scenarios of ground-based

microwave radiometers. The core contribution of this study is the construction of a small-scale joint prior experience database for temperature and relative humidity. This effectively overcomes the excessive reliance of traditional methods on large amounts of historical training data. Additionally, the robustness and accuracy of retrieval results in dynamic marine environments have been enhanced. This was done by integrating a pressure-altitude model and a buoy attitude compensation mechanism.

Simulation experiments and field tests in the Jiaozhou Bay area have thoroughly validated the effectiveness and feasibility of this method. Notably, the comprehensive statistical analysis of the 38 validation cases demonstrates an overall RMSE of 2.08 K for temperature and 20.95% for relative humidity. The profiles were retrieved by the NSGA-II algorithm. This confirms the potential for high-precision retrieval of atmospheric profiles in marine regions with sparse sounding stations. The average profile comparison shown in Fig.6 indicates that the retrieved profiles generally align well with sounding observation data. This is particularly true near the surface and in the upper troposphere. However, some fluctuations and deviations exist in the middle troposphere (2-8 km). These are closely related to the detection mechanism of the microwave radiometer. Due to the low sensitivity of the atmospheric microwave weighting function in its valley region, the retrieval accuracy in the middle troposphere is easily challenged. This systematic deviation is consistent with the findings of Cimini et al. (2006), who attributed similar biases in this altitude range to uncertainties in the oxygen absorption model. Especially for water vapor, its rapid vertical changes and complex layered structure exceed the constraints of the limited prior experience database. This leads to significant fluctuations in the retrieval results in this region. However, overall, this method demonstrates significant potential for application.

However, due to the high cost and short window period of maritime synchronous sounding experiments, only 38 sets of valid matching profiles were obtained. The limited sample size restricts the extrapolation of results to larger marine areas and extreme weather conditions. Future work will focus on two areas: data fusion and the expansion of observation networks. First, by increasing the number of buoys deployed, a maritime observation network will be established. This will achieve broader and more precise monitoring of marine atmospheric parameters. Second, multi-source data fusion techniques will be actively explored. This involves combining buoy observation data with satellite microwave / GNSS remote sensing data. This not only alleviates data scarcity but also provides richer assimilation data for numerical weather forecasting, further enhancing marine meteorological forecasting capabilities. Additionally, transfer learning methods will be adopted to improve the model's generalizability further.

In terms of algorithm optimization, the atmospheric prior experience database and multi-objective optimization strategy (NSGA-II) provide preliminary and effective constraints. However, there is still room for further improvement. The constraints include boundary and interlayer constraints for the retrieval algorithm. Future research can explore the introduction of more comprehensive physical constraints. This will further reduce retrieval uncertainty and improve accuracy. Additionally, the settings of evolutionary parameters in the NSGA-II algorithm have a critical impact on convergence speed and global optimization capability. These parameters include the genetic operator and mutation operator. Subsequent work can employ

more systematic simulation optimization strategies to fine-tune these parameters. The aim is to achieve higher retrieval accuracy and computational efficiency.

6 Conclusion

This study addresses challenges posed by data sparsity and platform attitude in traditional marine atmospheric detection. An innovative method is proposed to retrieve tropospheric atmospheric parameter profiles. The core work and main conclusions are summarized as follows:

(1) A retrieval model independent of historical data was established: A small-scale joint prior experience database for temperature and relative humidity was innovatively constructed. This was based on limited historical sounding data and a pressure-height model. It provides reasonable boundary constraints for subsequent retrieval algorithms. This mechanism effectively overcomes the reliance of traditional methods on massive historical data. It offers a solution for marine environments where data acquisition is challenging.

(2) Development and validation of a retrieval model based on a multi-objective genetic algorithm: A convective tropospheric temperature and humidity profile co-retrieval method was proposed. This method is based on a multi-objective genetic algorithm (NSGA-II). It integrates the microwave radiometer observed brightness temperature with physical constraints into a multi-objective optimization problem. It also significantly improves retrieval efficiency through parallel computation optimization. Field sea trial results demonstrate that this method can achieve high-precision temperature and humidity profile retrieval. The RMSE values are 2.08 K for temperature and 20.95 % for relative humidity. This provides an effective solution for data-scarce marine environments.

(3) Integrated application of microwave radiometers on buoy platforms was achieved: Ground-based microwave radiometers were successfully integrated with buoy platforms. Changes in zenith angle caused by buoy sway were compensated for using attitude sensors. This effectively improved the accuracy of marine observations. This integrated innovative method provides a new technical approach for meteorological detection in mesoscale marine regions. This is particularly useful in marine areas with sparse traditional sounding stations. It enables real-time, continuous atmospheric monitoring.

Overall, the method proposed in this study provides new insights into addressing the challenges of tropospheric atmospheric parameter detection in marine environments. Future research will continue to focus on three areas: the refinement and optimization of algorithms, multi-source data fusion, and the expansion of observation networks. The aim is to further enhance the model's universality and application value.

Author contribution

Zhiqian Li was responsible for conceptualization, methodology, software (model code development), data curation, and validation. He also wrote the original draft with support from all co-authors. Fuqing Liu contributed to the investigation

(experimental execution) and data curation, and participated in the review and editing of the manuscript. She also performed a critical review and editing of the manuscript. Shuo Jiang, Zhongling Zhou, Zhijin Qiu, Jing Zou, Tong Hu, and Ke Qi contributed to the investigation (field experiments) and provided essential resources and technical support. Bo Wang was responsible for project management, fundraising, reviewing and editing. Bin Wang was also responsible for project management, reviewing and editing.

Competing interests

The authors declare that they have no conflict of interest. Disclaimer

Acknowledgements

The authors thank the University of Wyoming for providing the radiosonde data.

Code and data availability

The source code, sea-trial observational dataset, and processing scripts related to this paper have been uploaded to Zenodo under a CC-BY-4.0 license (https://doi.org/10.5281/zenodo.17389912). The runtime environment is Python 3.9. Historical radiosonde data were obtained from the University of Wyoming public database (Qingdao station, ID 54857) and are freely available at http://weather.uwyo.edu/upperair/bufrraob.shtml.

Financial support

This study was financially supported by the National Key R&D Program of China (Grant no. 2022YFC3104202), the National Natural Science Foundation of China (Grant nos. 42206188 and 42176185), the Shandong Provincial Key R&D Program (Competitive Platform) (Grant nos. 2023CXPT015), the National Cooperation Special Project for Science, Education, and Industry Integration Pilot Program: Research on Digital Twin System for Atmospheric Waveguides in the Yellow and Bohai Sea (Grant nos. 2024GH05), the Major Innovation Projects of the Science-Education-Industry Integration Pilot Program: the Development and Application Demonstration of a Shipborne Lidar-Based Marine Atmospheric Duct Detection System (Grant nos. 2025ZDZX05) and Research Development and Demonstration of Key Technologies and Equipment for Intelligent Calibration and Validation of Ocean Satellite Remote Sensing (Grant nos. 2025ZDYS01), the Major Scientific Research Project for the Construction of State Key Laboratory at Qilu University of Technology (Shandong Academy of Sciences) (Grant nos. 2025ZDGZ01).

Review statement

References

Maciejewska, A.: Use of Tropospheric Delay in GNSS-Based Climate Monitoring—A Review, Remote Sensing, 17, 1501-1529, https://doi.org/10.3390/rs17091501, 2025.

Morbidelli, R., Corradini, C., Saltalippi, C., and Flammini, A.: Atmospheric Stability and Meteorological Scenarios as Inputs to Air Pollution Transport Modeling, Water Air & Soil Pollution, 218, 275-281, https://doi.org/10.1007/s11270-010-0640-5, 2011.

Guimond, S. R., Zhang, J. A., Sapp, J. W., and Frasier, S. J.: Coherent Turbulence in the Boundary Layer of Hurricane Rita (2005) during an Eyewall Replacement Cycle, Journal of the Atmospheric Sciences, 75, 3071-3093, https://doi.org/10.1175/JAS-D-17-0347.1, 2018.

Ahern, K., Bourassa, M. A., Hart, R. E., Zhang, J. A., and Rogers, R. F.: Observed Kinematic and Thermodynamic Structure in the Hurricane Boundary Layer During Intensity Change, Monthly Weather Review, 147, https://doi.org/10.1175/MWR-D-18-0380.1 2019.

Wei, C., Zhao, X., Zhu, X., Yang, P., Liu, Y., Chen, Y., and Wang, D.: Vertical wind shear induced asymmetry on atmospheric duct distribution in the context of tropical cyclones, Science China Earth Sciences, https://doi.org/10.1007/s11430-025-1660-1, 2025.

Cimini, D., Haeffelin, M., Kotthaus, S., Löhnert, U., Martinet, P., O'Connor, E., Walden, C., Collaud Coen, M., and Preissler, J.: Towards the profiling of the atmospheric boundary layer at European scale—introducing the COST Action PROBE, *Bulletin of Atmospheric Science and Technology*, 1, 23–42, https://doi.org/10.1007/s42865-020-00003-8, 2020.

Roemmich, D., Johnson, G. C., Riser, S., Davis, R., Gilson, J., Owens, W. B., Garzoli, S. L., Schmid, C., and Ignaszewski, M.: The Argo Program: Observing the Global Ocean with Profiling Floats, Oceanography, 22, 34-43, https://doi.org/10.5670/oceanog.2009.36, 2009.

Clough, S. A., Shephard, M. W., Mlawer, E. J., Delamere, J. S., Iacono, M. J., Cady-Pereira, K., Boukabara, S., and Brown, P. D.: Atmospheric radiative transfer modeling: a summary of the AER codes, Journal of Quantitative Spectroscopy and Radiative Transfer, 91, 233-244, https://doi.org/10.1016/j.jqsrt.2004.05.058, 2005.

Hewison, T. J.: 1D-VAR Retrieval of Temperature and Humidity Profiles From a Ground-Based Microwave Radiometer, IEEE Transactions on Geoscience & Remote Sensing, 45, 2163-2168, https://doi.org/10.1109/TGRS.2007.898091, 2007.

Zhou, S., Wei, Y., Lu, P., Yu, G., Wang, S., Jiao, J., Yu, P., and Zhao, J.: A Deep Learning Gravity Inversion Method Based on a Self-Constrained Network and Its Application, Remote Sensing, 16, 995-1010, https://doi.org/10.3390/rs16060995, 2024.

Liu, W., Wang, H., Xi, Z., and Wang, L.: Physics-Informed Deep Learning Inversion with Application to Noisy Magnetotelluric Measurements, Remote Sensing, 16, 62-82, https://doi.org/10.3390/rs16010062, 2024.

Gaffard, C. and Hewison, T.: Radiometrics MP3000 Microwave Radiometer Trial Report, http://tim.hewison.org/TR26.pdf, 2003.

Reinhardt, C., Kuga, Y., Jaruwatanadilok, S., and Ishimaru, A.: Improving bit-error-rate performance of the free-space optical communications system with channel estimation based on radiative transfer theory, IEEE Journal on Selected Areas in Communications, 27, 1591-1598, https://doi.org/10.1109/JSAC.2009.091209, 2009.

Zheng, S.: Ocean duct inversion from radar clutter using variation adjoint and regularization method (II): inversion experiment, Acta Physica Sinica,59,3912, https://doi.org/10.7498/aps.59.3912, 2010.

Renju, R., Raju, C. S., Swathi, R., and Milan, V. G.: Retrieval of atmospheric temperature and humidity profiles over a tropical coastal station from ground-based Microwave Radiometer using deep learning technique, Journal of Atmospheric and Solar-Terrestrial Physics, 249,106094, https://doi.org/10.1016/j.jastp.2023.106094, 2023.

Hu, J., Wu, J., Petropoulos, G. P., Bao, Y., Liu, J., Lu, Q., Wang, F., Zhang, H., and Liu, H.: Temperature and Relative Humidity Profile Retrieval from Fengyun-3D/VASS in the Arctic Region Using Neural Networks, Remote Sensing, 15, 1648, https://doi.org/10.3390/rs15061648, 2023.

Jiménez, C. and Eriksson, P.: A neural network technique for inversion of atmospheric observations from microwave limb sounders, Radio Science, 36, 941-953, https://doi.org/10.1029/2000RS002561, 2016.

Yao, S. and Guan, L.: Comparison of Three Convolution Neural Network Schemes to Retrieve Temperature and Humidity Profiles from the FY4A GIIRS Observations, Remote Sensing, 14, 5112, https://doi.org/10.3390/rs14205112, 2022.

Mahdianpari, M., Ghanbari, H., Mohammadimanesh, F., and Homayouni, S.: A Meta-Analysis of Convolutional Neural Networks for Remote Sensing Applications, IEEE Journal of Selected Topics in Applied Earth Observations and Remote Sensing, 14, 3602-3613, https://doi.org/10.1109/JSTARS.2021.3065569, 2021.

Turner, D. D., Clough, S. A., Liljegren, J. C., Clothiaux, E. E., and Gaustad, K. L.: Retrieving Liquid Wat0er Path and Precipitable Water Vapor From the Atmospheric Radiation Measurement (ARM) Microwave Radiometers, IEEE Transactions on Geoence and Remote Sensing, 45, 3680-3690, https://doi.org/10.1109/TGRS.2007.903703, 2007.

Decker, M. T., Westwater, E. R., and Guiraud, F. O.: Experimental Evaluation of Ground-Based Microwave Radiometric Sensing of Atmospheric Temperature and Water Vapor Profiles, Journal of Applied Meteorology, 17, 1788-1795, https://doi.org/10.1175/1520-0450(1978)017%3C1788:EEOGBM%3E2.0.CO;2, 1978.

Guiraud, F. O., Howard, J., and Hogg, D. C.: A Dual-Channel Microwave Radiometer for Measurement of Precipitable Water Vapor and Liquid, IEEE Transactions on Geoscience Electronics, 17, 129-136, https://doi.org/10.1109/TGE.1979.294639, 1979.

Candlish, L. M., Raddatz, R. L., Asplin, M. G., and Barber, D. G.: Atmospheric Temperature and Absolute Humidity Profiles over the Beaufort Sea and Amundsen Gulf from a Microwave Radiometer, Journal of Atmospheric & Oceanic Technology, 29, 1182-1201, https://doi.org/10.1175/JTECH-D-10-05050.1, 2012.

Wei, C., Zhao, X., Liu, Y., Yang, P., Zhou, Z., and Chen, Y.: Bias Analysis and Correction of ERA5 Reanalysis in the Context of Tropical Cyclones, Journal of Geophysical Research: Atmospheres, 130, https://doi.org/10.1029/2024JD042737, 2025.

批注 [滴滴61]: Thank you for pointing this out. In the revised manuscript (Page 23, Line 603), "Wat0er" has been corrected to "Water".
(RC2, Line 489)

Schnitt, S., Foth, A., Kalesse-Los, H., Mech, M., Acquistapace, C., Jansen, F., Löhnert, U., Pospichal, B., Röttenbacher, J., Crewell, S., and Stevens, B.: Ground- and ship-based microwave radiometer measurements during EUREC4A, Earth Syst. Sci. Data, 16, 681–700, https://doi.org/10.5194/essd-16-681-2024, 2024.

Cronin, M. F., Anderson, N. D., Zhang, D., Berk, P., Wills, S. M., Serra, Y., Kohlman, C., Sutton, A. J., Honda, M. C., and Kawai, Y.: PMEL Ocean Climate Stations as Reference Time Series and Research Aggregate Devices, Oceanography, 36, 8, https://doi.org/10.5670/oceanog.2023.224, 2023.

Liu, L., Liao, Z., Chen, C., Chen, J., and Liu, T.: A Seabed Real-Time Sensing System for In-Situ Long-Term Multi-Parameter Observation Applications, Sensors, 19, 1255, https://doi.org/10.3390/s19051255, 2019.

Fang, H., Callafon, R. A., and Cortés, J.: Estimation-Based Ocean Flow Field Reconstruction Using Profiling Floats, Offshore Mechatronics Systems Engineering, https://doi.org/10.1201/9781315185378-8, 2018.

Haun, E.: World's First Floating Microwave Radiometer, Marine Technology News, available at: https://www.marinetechnologynews.com/news/world-first-floating-microwave-544561 (last access: 22 November 2025), 2017.

Griesche, H. J., Seifert, P., Ansmann, A., Baars, H., Barrientos Velasco, C., Bühl, J., Engelmann, R., Radenz, M., Zhenping, Y., and Macke, A.: Application of the shipborne remote sensing supersite OCEANET for profiling of Arctic aerosols and clouds during Polarstern cruise PS106, Atmos. Meas. Tech., 13, 5335–5358, https://doi.org/10.5194/amt-13-5335-2020, 2020.

Yan, H., Zhao, Y., and Chen, S.: An Improved 1D-VAR Retrieval Algorithm of Temperature Profiles from an Ocean-Based Microwave Radiometer, J. Mar. Sci. Eng., 10, 641, https://doi.org/10.3390/jmse10050641, 2022.

Cimini, D., Gandoin, R., Fiedler, S., Acquistapace, C., Balotti, A., Gentile, S., Geraldi, E., Knist, C., Martinet, P., Nilo, S. T., Pace, G., Pospichal, B., and Romano, F.: Atmospheric stability from numerical weather prediction models and microwave radiometer observations for onshore and offshore wind energy applications, Atmos. Meas. Tech., 18, 2041–2067, https://doi.org/10.5194/amt-18-2041-2025, 2025.

Cimini, D., Shaw, J. A., Han, Y., Westwater, E. R., Irisov, V., Leuski, V., and Churnside, J. H.: Air temperature profile and air-sea temperature difference measurements by infrared and microwave scanning radiometers, Radio Sci., 38, 8045, https://doi.org/10.1029/2002RS002632, 2003.

China Electronics Technology Group Corporation No.22 Research Institute (CETC-22): User Manual for QFW-6000 Ground-based Microwave Radiometer, Qingdao, China, 2022.

Zhang, Q., Deng, B., Wang, S., Dong, F., and Shao, M.: Multi-Source Retrieval of Thermodynamic Profiles from an Integrated

Tu, M., Zhang, W., Bai, J., Wu, D., Liang, H., and Lou, Y.: Spatio-Temporal Variations of Precipitable Water Vapor and Horizontal Tropospheric Gradients from GPS during Typhoon Lekima, Remote Sensing, 13, 4082, 2021.

ITU-R: Recommendation ITU-R P.676-13: Attenuation by atmospheric gases and related effects, P Series, International Telecommunication Union, Geneva, 2022.

Rosenkranz, P. W.: Water vapor microwave continuum absorption: A comparison of measurements and models, Radio Sci., 33, 919–928, https://doi.org/10.1029/98RS01182, 1998.

National Energy Administration of China: Code for Design of Combustion System of Fossil Fired Power Plant (DL/T 5240-2010), China Electric Power Press, Beijing, 2010.

Kim, H.-Y.: Statistical notes for clinical researchers: assessing normal distribution (2) using skewness and kurtosis, Restor. Dent. Endod., 38, 52–54, https://doi.org/10.5395/rde.2013.38.1.52, 2013.

International Telecommunication Union (ITU). P.676: Attenuation by atmospheric gases and related effects. 2022. ITU. Available at: https: //www. itu. int/rec/R-REC-P. 676-13-202208-I/en.

Deb, K., Pratap, A., Agarwal, S., and Meyarivan, T.: A fast and elitist multiobjective genetic algorithm: NSGA-II, IEEE Transactions on Evolutionary Computation, 6, 182-197, 2002.

WMO: Guide to Meteorological Instruments and Methods of Observation, WMO-No. 8, World Meteorological Organization, Geneva, 2018.

Sun, J., Xue, M., Wilson, J. W., Zawadzki, I., Ballard, S. P., Onvlee-Hooimeyer, J., Joe, P., Barker, D. M., Li, P. W., and Golding, B.: Use of NWP for Nowcasting Convective Precipitation: Recent Progress and Challenges, Bulletin of the American Meteorological Society, 95, 409-426, 2014.

Cimini, D., Hewison, T. J., Martin, L., Güldner, J., Gaffard, C., and Marzano, F. S.: Temperature and humidity profile retrievals from ground-based microwave radiometers during TUC, Meteorologische Zeitschrift, 15, 45–56, https://doi.org/10.1127/0941-2948/2006/0099, 2006.

Massaro, G., Stiperski, I., Pospichal, B., Rotach, M., and W.: Accuracy of retrieving temperature and humidity profiles by ground-based microwave radiometry in truly complex terrain, Atmospheric Measurement Techniques Discussions, 2015.

Yan, X., Liang, C., Jiang, Y., Luo, N., and Li, Z.: A Deep Learning Approach to Improve the Retrieval of Temperature and Humidity Profiles From a Ground-Based Microwave Radiometer, IEEE T. Geosci. Remote, 58, 7827–7836, https://doi.org/10.1109/TGRS.2020.2984432, 2020.

Cimini, D., Campos, E., Ware, R., Albers, S., Giuliani, G., Oreamuno, J., Joe, P., Koch, S. E., Cober, S., and Westwater, E.: Thermodynamic Atmospheric Profiling During the 2010 Winter Olympics Using Ground-Based Microwave Radiometry, IEEE Transactions on Geoscience & Remote Sensing, 49, 4959-4969, 2011.

批注 [滴滴62]: The reference list has been updated by adding and removing relevant references and by reordering them to match the revised in-text citations (Referee #1).